33rd Annual International Conference of the IEEE EMBS
Boston, Massachusetts USA, August 30 - September 3, 2011

Automated Cavity Detection of Infectious Pulmonary Tuberculosis in Chest Radiographs

Tao Xu, Irene Cheng, *Senior Member IEEE*, and Mrinal Mandal, *Senior Member, IEEE*

***Abstract*—The presence of cavities in the upper lung zones is an important indicator of highly infectious Tuberculosis (TB). Diagnoses performed by the radiologists are labor intensive and of high inter-reader variation. After analyzing the existing computer-aided detection techniques, we propose an fully automated TB cavity detection system which combines a 2D Gaussian-model-based template matching (GTM) for candidates detection with Hessian-matrix-based image enhancement (HIE) for the following cavity segmentation and feature extraction. Experimental results demonstrate that our approach outperforms the existing TB cavity detection technique with higher accuracy and lower false positive rate.**

I. Introduction

DUE to its advantages such as noninvasive characteristic, lower radiation dose and lower cost than CT, and wide availability, chest radiography remains the most commonly used procedure to diagnose respiratory diseases in a typical radiology department [1]. Given the shortage of radiologists compared to a huge amount of chest radiographs or chest X-ray (CXR) images to be examined, a computer-aided detection/diagnosis (CAD) system is necessary to reduce the work of radiologists. On the other hand, tuberculosis (TB), especially infectious TB, such as post-pulmonary (reactivation) TB and HIV-related TB continues to be a public health problem of global proportions, especially in developing countries [2]. Although chest radiography is increasingly important in the fight against TB, the sensitivity (70%-80%) and specificity (60%-70%) of radiologists' diagnosis using conventional chest radiography are low and inter-reader variation is high [3]. CAD systems can pave the way for the automated or semi-automated diagnostic interpretation of chest radiographs.

The overwhelming majority of chest radiography CAD applications has focused on lung nodule detection. Less work has been done in CAD development for TB. Existing CAD schemes using texture features for interstitial disease diagnosis can be treated as TB-related [4]. However, those interstitial changes are not typical radiographic findings of the infectious TB. Cavitation (cavity formation) in the upper lung zones is an important characteristic of post-primary TB, and it is an indicator that disease has developed into a state of high infectivity [3]. Since the radiographic manifestations of HIV-related TB are more complicated (depending on the degree of immunosuppression), our current research only focuses on the cavity detection of post-primary TB.

To the best of our knowledge, only one effort for TB cavity detection has been made based on a hybrid knowledge-based framework [5], which mainly includes: 1) manually upper lung zone extraction step, 2) image enhancement step using mean shift technique, 3) cavity candidates detection step using adaptive thresholding, 4) candidate contour segmentation step using snake-based technique, and 5) contour's geometric and photometric features extraction step for the final cavity classification. One limitation of this CAD system is the parameters sensitivity of mean shift clustering due to cavity's size variation and disturbing effects of its neighboring superimposed anatomical structures. The other limitation comes from the training dataset and manual operation which make the system much more supervised. To overcome these problems, we propose a new TB cavity detection system using a 2D Gaussian- model-based template matching (GTM) for automated candidate detection and the Hessian-matrix-based image enhancement (HIE) for the later contour segmentation and feature extraction steps.

The rest of this paper is organized as follows: Section II provides the details of the proposed cavity detection system. Experimental results are demonstrated in Section III, followed by Section IV in which conclusions are discussed.

II. Methods

The proposed TB cavity detection system for an input CXR image contains four modules: GTM, HIE, segmentation, feature extraction and classification (See Fig. 1).

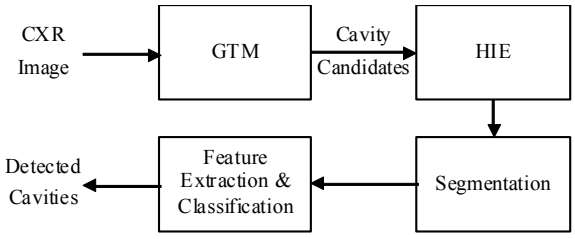

Fig. 1. Schematic of the proposed CAD system for infectious TB cavity detection. GTM: Gaussian-model-based template matching. HIE: Hessian-matrix-based image enhancement.

A. Gaussian-model-based Template Matching

Template matching (TM) has been a useful and familiar

Manuscript received on April 15th, 2011.

Tao Xu is with the Dept. of Electrical and Computer Engineering, University of Alberta , Edmonton, AB, T6G 2V4 CA (e-mail: tx1@ualberta.ca). Irene Cheng is with the Dept. of Computing Science, University of Alberta, Edmonton, AB T6G 2E8 CA (e-mail: locheng@ualberta.ca). Corresponding Author: Mrinal Mandal is also with the Dept. of Electrical and Computer Engineering, University of Alberta , Edmonton, AB, T6G 2V4 CA (e-mail: mandal@ece.ualberta.ca)

tool for pattern recognition. Traditional TM involves the translation of a given template to every possible position in the test image and a similarity measure of the match between the template and template-sized subimage at that position. Normalized cross correlation is usually used as the measure of similarity, due to its speed-up implementation using fast Fourier transform (FFT), integral images or bounded partial correlation. Since traditional TM is sensitive to object's rotation and scale variance, three major types of rotation and scale invariant TM techniques have been considered: 1) Based on a set of template images with various object sizes and angles [6]; 2) Based on rotation and scale invariant transform, e.g. Fourier-Mellin transform, or ring-projection transform [7]; 3) Based on vector subspace of various template images. The subspace is spanned by major eigenvectors using Karhunen-Loeve transform, or tangent vectors [8]. Techniques of type 2) and 3) can only handle with object's small distortion, thus, we use similar idea of type 1) for cavity candidates detection.

Artificial template images' generation is based on the knowledge of cavity. A cavity is defined as a parenchymal cyst greater than 1cm in diameter, containing either air or fluid or both [3]. Since cavities are created by tissue necrosis within nodules or masses, their radiographic patterns are usually annular rings with variable wall thickness. Fig. 2 (a) is a CXR image with a typical cavity in the patient's upper left lung zone. In a local region which contains the whole cavity, line-cut intensity plots in different directions appear similar. (See Fig. 2 (b).) Therefore, we propose to mimic the pattern using 2D circular or elliptical Gaussian ring distribution. The generic 2D Gaussian ring is defined as:

$$I(x,y) = e^{-\left[(x-wx)^2+(y-wy)^2\right]/2\sigma^2} \qquad (1)$$

where $w = \dfrac{ab}{\sqrt{a^2y^2+b^2x^2}}$, a and b are the major and minor axes, $I(x,y)$ is the image intensity function in the 2D domain, and σ is the standard deviation of the Gaussian distribution which determines the wall thickness of the ring. Noting that

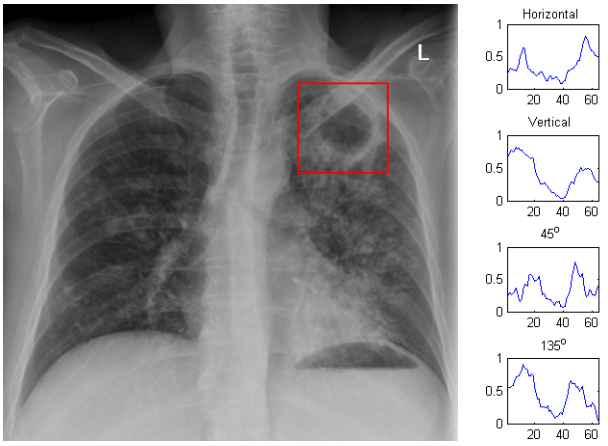

(a) (b)

Fig. 2. (a) A CXR image with a typical cavity; (b) Line-cut intensity plots of 4 directions in local cavity region.

when $a = b = r$, Eq. (1) is the specific case of 2D circular Gaussian ring, where r is the inner radius. Based on Eq. (1), we could build template images for matching with various sizes and wall thicknesses by changing the value of a, b and σ. And the rotation angle θ can be incorporated using the following coordinates substitution:

$$\begin{cases} x = x'\cos\theta + y'\sin\theta \\ y = y'\cos\theta - x'\sin\theta \end{cases}. \qquad (2)$$

Given a 512×512 CXR image, its pixel spacing is [0.8mm 0.8mm], which means the physical size is 409.6mm × 409.6mm. Since the diameter of the largest cavity is usually less than 6 cm and the wall thickness is within the range of [4mm, 16mm], we define the template size as 75×75. Fig. 3 shows template images with various radii, rotation angle and wall thickness.

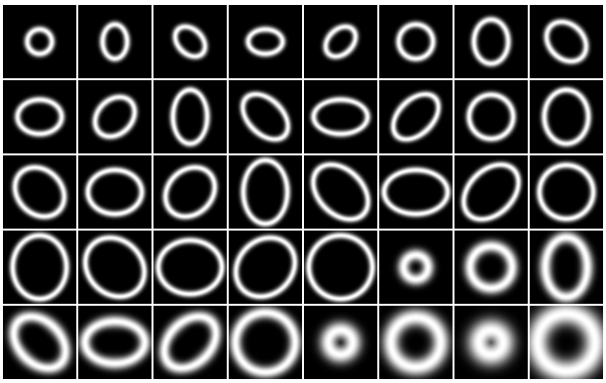

Fig. 3. An example of cavity template database. a/b<1.6, wall thickness within [5,20], and θ=0°,45°,90°,135°.

B. Hessian-matrix-based Image Enhancement

By thresholding the NCC obtained from the set of templates above, the GTM could locate the suspicious cavities in a bunch of candidates. Before applying the edge-based segmentation for shape extraction, image enhancement is necessary for preserving the strong edges related to cavity and suppressing other noises. Multi-scale analysis of the Hessian matrix has been widely used for local patterns such as plate-like, line-like or blob-like structures' enhancement [9]. In this frame work, the 2nd derivatives of a Gaussian smoothed image is defined as a convolution between the original image and the derivatives of Gaussians:

$$\begin{cases} L_{xx}(x,y,\sigma) = \sigma^2 I(x,y) * G_{xx}(x,y,\sigma) \\ L_{xy}(x,y,\sigma) = \sigma^2 I(x,y) * G_{xy}(x,y,\sigma) \\ L_{yy}(x,y,\sigma) = \sigma^2 I(x,y) * G_{yy}(x,y,\sigma) \end{cases} \qquad (3)$$

where L is the smoothed image at point (x,y) with scale σ, I is the original image, and G stands for the Gaussian kernel. The intrinsic characteristic of this analysis is that the 2nd derivative of a Gaussian kernel at scale σ generates a probe kernel that measures the contrast between the regions inside and outside the range $(-\sigma, \sigma)$ in the direction of the derivative (See Fig. 4 for an 1D example). One known problem of this kind of method is that too much blurring occurred during the

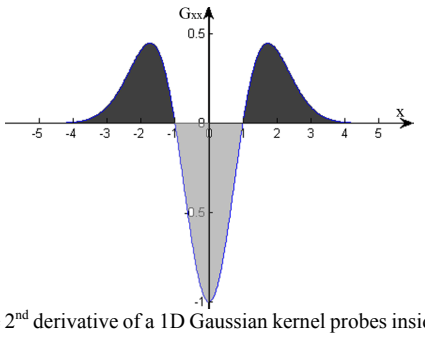

Fig. 4. The 2nd derivative of a 1D Gaussian kernel probes inside/outside contrast of the range (-σ, σ). In this example, σ=1.

multiscale smoothing may lead to false detections [10]. Therefore, for a candidate image, we calculate its object scale k (proposed by Saha et al. [11]) as its σ. The corresponding Hessian matrix is:

$$H_k = \begin{bmatrix} L_{xx}(x,y,k) & L_{xy}(x,y,k) \\ L_{yx}(x,y,k) & L_{yy}(x,y,k) \end{bmatrix}. \quad (4)$$

And its eigenvalues are λ_1 and λ_2 ($|\lambda_1| \geq |\lambda_2|$). By exploiting those eigenvalues, we found that the annular ring-like structure could be greatly enhanced using the following equation:

$$I_{enhanced} = I \cdot |\lambda_1|. \quad (5)$$

Middle row images in Fig. 5 (a) and (b) give some enhanced results of both cavity and noncavity candidate images.

C. Segmentation

Based on the HIE results, our previous proposed improved fluid vector flow (IFVF) [12] is applied for fast and accurate shape extraction. Comparing to the existing edge-based Snake models, IFVF generates the external force dynamically and has the largest capture range. The traditional Snake model, which converts the parametric curve evolution into an energy minimization problem, can be treated as a force balance equation:

$$F_{\text{int}}(v) + F_{ext}(v) = 0 \quad (6)$$

where F_{int} is the internal force constraining the smoothness of contour v, and F_{ext} is the external force attracting the contour toward image features. The external force of IFVF contains both static and dynamic terms. The static forces calculated from the image remain unchanged as the snake deforms while the dynamic forces dependent on the snake change as the snake deforms.

$$F_{\text{IFVF}} = F_{\text{static}} + F_{\text{dynamic}} \quad (7)$$

F_{static} could be any static external forces which overcomes the edge leakage problem, and F_{dynamic} is described as follows:

$$F_{\text{dynamic}} = (1-f)\delta \frac{\nabla d'(x,y)}{\|\nabla d'(x,y)\|} \quad (8)$$

where f is image's edge map, $\delta = \pm 1$ controls the inward or outward direction, and d' is the Euclidean distance between any point (x,y) on the image plane and the new defined control point using Hausdorff distance [12]. The bottom rows in Fig. 5 (a) and (b) are the IFVF segmentation results.

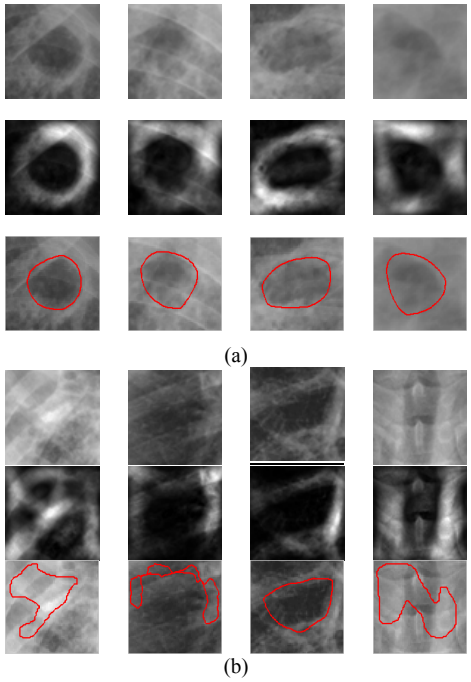

Fig. 5. (a) Top Row: candidate images with cavity; Middle Row: corresponding HIE results, Bottom Row: segmentation results; (b) Top Row: candidate images without cavity; Middle Row: corresponding HIE results, Bottom Row: segmentation results.

D. Feature Extraction and Classification

Since HIE significantly helps the accurate shape extraction, only geometric feature such as circularity need to be extracted. The classification of cavity is then finished by the circularity thresholding.

III. Results

Standard posteroanterior (PA) chest radiographs from two different databases (normal and abnormal) are chosen as the experimental materials: 1) a publicly available Japanese Society of Radiological Technology (JSRT) database [13]; 2) a CXR image database from the University of Alberta Hospital. Images are grouped into three sets: 20 from CXR database as the cavity set , 20 from the CXR database as the noncavity set, and 20 from the JSRT database as the normal set. All images were read independently by three experienced chest radiologists, who are specialized in TB diagnosis. When the interpretations of an image were different between the radiologists, they reanalyzed the image and came to a consensus. The presence of TB cavities in an image was confirmed by the radiologists. Performance of our proposed TB detection system is evaluated in two parts:

A. Performance of Cavity Detection

Given an image dataset with n images, four parameters including true positive rate (TPR), false positive rate (FPR), missing rate (MR) and false positive rate per image (FPRPI) are used to evaluate the cavity detection performance:

$$\text{TPR}=\frac{\#\text{of true cavities detected}}{\text{Total \#of cavities detected}}\times 100\%$$
$$\text{MR}=\frac{\#\text{of true cavities undetected}}{\text{Total \#of true cavities}}\times 100\% \qquad (9)$$
$$\text{FPRPI}=\frac{1}{n}\sum_{i=1}^{n}\frac{\#\text{of false cavities detected}}{\text{Total \#of cavities detected}}\times 100\%$$
$$\text{FPR}=1-\text{TPR}$$

TABLE I shows the cavity candidates detection results between our proposed method and the hybrid method in [5]. It could be found that the proposed method outperforms the existing technique in all the indices. For example, in the cavity set (20 CXR images containing 26 cavities), our proposed CAD system has over 13% increment of TPR. Meanwhile, FPR, MR and FPRPI are decreased almost 13%, 4% and 6%, respectively. For CXR images of normal or abnormal lungs without cavity, our approach also lower the FPRPI significantly.

TABLE I
CAVITY DETECTION RESULTS

Methods	IMG	#C	#D	TPR	FPR	MR	FPRPI
Hybrid [5]	CS	26	33	54.5%	45.5%	30.8%	35.2%
	NCS	0	14	n/a	n/a	n/a	70.0%
	NS	0	5	n/a	n/a	n/a	25.0%
Proposed	CS	26	28	67.9%	32.1%	26.9%	29.6%
	NCS	0	10	n/a	n/a	n/a	50.0%
	NS	0	4	n/a	n/a	n/a	20.0%

CS, NCS and NS are the abbr. of three datasets: cavity set, noncavity set and normal set. #C stands for the number of true cavities, which indicates the ground truth. #D stands for the number of final detected cavities. n/a: TPR, FPR, and MR are not applicable in the image dataset without cavities.

B. Segmentation

Overlapping degree Ω was used for cavity segmentation evaluation. For those candidates with cavities, assuming the contour manually outlined by the radiologist as the ground truth, the overlapping degree between ground truth A and contour B obtained by using IFVF is defined as follows:

$$\Omega=\frac{\mathbf{A}\bigcap\mathbf{B}}{\mathbf{A}\bigcup\mathbf{B}} \qquad (10)$$

where **A** and **B** are the sets of all pixels enclosed by contours A and B. The segmentation results with and without HIE are compared in TABLE II, where μ, σ and median are the expected value, standard deviation and median value of Ω, respectively. It can be seen that with the help of HIE, the segmentation accuracy is improved almost 8% considering both mean and median. Noting that due to HIE's promising filtering result, segmentation results of other edge-based Snake models would be quite similar.

TABLE II
SEGMENTATION EVALUATION

IFVF	μ	σ	median
Without HIE	68.8%	5.9%	69.0%
With HIE	77.2%	5.7%	76.9%

IV. CONCLUSIONS

In this paper, we propose a computer-aided system for TB cavity detection from chest radiographs. Without changing any information of the original image, a GTM is applied to find the cavity candidates. The HIE technique then improves the image quality for the following segmentation and feature extraction. Final classification results indicate that the proposed system has better detection performance than the previous technique. Furthermore, the detection will be much more accurate if it is combined with automatic lung field segmentation techniques.

ACKNOWLEDGMENT

The authors would like to thank Dr. Richard Long, TB Research Center, University of Alberta, for providing the post-primary TB image dataset and for helpful discussions.

REFERENCES

[1] H.P. McAdams, E. Samei, J. Dobbins III, et al, "Recent advances in chest radiography," *Radiology*, 2006, 241(3), pp. 663-83.

[2] World Health Organization, "Epidemiology," in *Global Tuberculosis Control: Epidemiology, Strategy, Financing*, Geneva, Switzerland: WHO Press, 2009, pp. 6-33.

[3] R. Long, E. Ellis, et al, *Canadian tuberculosis standards (6th ed.)*, Public Health Agency of Canada, 2007.

[4] B.V. Ginneken, L. Hogeweg, and M. Prokop, "Computer-aided diagnosis in chest radiography: beyond nodules," *European Journal of Radiology*, 2009, 72(2), pp. 26-30.

[5] R. Shen, I. Cheng, and A. Basu, "A hybrid knowledge-guided detection technique for screening of infectious pulmonary tuberculosis from chest radiographs," *IEEE Trans. on Biomedical Engineering*, 2010, 57(11), pp. 2646-2656.

[6] T. Hara, H. Fujita, et al, "Automated lesion detection methods for 2D and 3D chest X-ray images", *Proceeding of Image Analysis and Processing Conference*, 1999, pp. 768-773.

[7] Y.H. Lin, C.H. Chen, "Template matching using the parametric template vector with translation, rotation and scale invariance," *Pattern Recognition*, 2008, 41(7), pp.2413-2421.

[8] B. Wohlberg, K. Vixie, "Invariant template matching with tangent vectors," *Optical Engineering*, 2007, 46(3), pp. 037006.

[9] Y. Sato, S. Nakajima, et al, "3D multiscale line filter for segmentation and visualization of curvilinear structure in medical images," *Med. Image Anal*, 1998, 2, pp. 143-168.

[10] J. Liu, J.M. White, and R.M. Summers, "Automated detection of blob structures by Hessian analysis and object scale," *Proceedings of ICIP*, 2010, pp. 841-844.

[11] P.K. Saha, and J.K. Udupa, "Scale-based image filtering preserving boundary sharpness and fine structure," *IEEE Trans. on Medical Imaging*, 2001, 20, pp. 1140-1155.

[12] T. Xu, I. Cheng, and M.K. Mandal, "An Improved Fluid Vector Flow for Cavity Segmentation in Chest Radiographs," *Proceedings of ICPR*, 2010, pp. 3376-3379.

[13] (2010. Nov.) Japanese Society of Radiological Technology [Online]. Available: http://www.jsrt.or.jp/english.html.